

JGR Atmospheres

-

RESEARCH ARTICLE

10.1029/2023JD039453

Key Points:

- The proposed model is highly effective in modeling thawing depth at higher time resolution and representing the soil energy budget
- Non-gradient models demonstrate a strong capability to model soil energy budget in data-sparse harsh environments

Correspondence to:

M. Zhu and J. Wang, modizhu@gatech.edu; jingfeng.wang@ce.gatech.edu

Citation:

Zhu, M., Wang, J., Ivanov, V., Sheshukov, A., Zhou, W., Zhang, L., et al. (2024). An analytical model of active layer depth under changing ground heat flux. *Journal of Geophysical Research: Atmospheres*, 129, e2023JD039453. https://doi.org/10.1029/2023JD039453

Received 12 JUN 2023 Accepted 11 FEB 2024

Author Contributions:

Conceptualization: Modi Zhu,
Jingfeng Wang
Data curation: Valeriy Ivanov,
Aleksey Sheshukov, Wenbo Zhou,
Liujing Zhang, Valeriy Mazepa,
Alexandr Sokolov, Victor Valdayskikh
Formal analysis: Modi Zhu,
Jingfeng Wang
Funding acquisition: Jingfeng Wang,
Valeriy Ivanov
Investigation: Modi Zhu, Jingfeng Wang,
Valeriy Ivanov, Aleksey Sheshukov
Methodology: Modi Zhu, Jingfeng Wang

Project administration: Jingfeng Wang, Valeriy Ivanov, Valeriy Mazepa, Alexandr Sokolov Resources: Jingfeng Wang, Valeriy Ivanov, Aleksey Sheshukov, Wenbo Zhou, Liujing Zhang, Valeriy Mazepa, Alexandr Sokolov, Victor Valdayskikh

© 2024. The Authors.

Software: Modi Zhu

This is an open access article under the terms of the Creative Commons
Attribution-NonCommercial-NoDerivs
License, which permits use and
distribution in any medium, provided the original work is properly cited, the use is non-commercial and no modifications or adaptations are made.

An Analytical Model of Active Layer Depth Under Changing Ground Heat Flux

Modi Zhu¹, Jingfeng Wang¹, Valeriy Ivanov², Aleksey Sheshukov³, Wenbo Zhou², Liujing Zhang², Valeriy Mazepa⁴, Alexandr Sokolov⁵, and Victor Valdayskikh⁶

¹School of Civil and Environmental Engineering, Georgia Institute of Technology, Atlanta, GA, USA, ²Department of Civil and Environmental Engineering, University of Michigan, Ann Arbor, MI, USA, ³Department of Biological and Agricultural Engineering, Kansas State University, Manhattan, KS, USA, ⁴Institute of Plant and Animal Ecology, the Ural Branch of the Russian Academy of Sciences, Yekaterinburg, Russia, ⁵Arctic Research Station, Institute of Plant and Animal Ecology, the Ural Branch of the Russian Academy of Sciences, Labytnangi, Russia, ⁶Ural Federal University, Yekaterinburg, Russia

Abstract Improved modeling of permafrost active layer freeze-thaw plays a crucial role in understanding the response of the Arctic ecosystem to the accelerating warming trend in the region over the past decades. However, modeling the dynamics of the active layer at diurnal time scale remains challenging using the traditional models of freeze-thaw processes. In this study, a physically based analytical model is formulated to simulate the thaw depth of the active layer under changing boundary conditions of soil heat flux. Conservation of energy for the active layer leads to a nonlinear integral equation of the thaw depth using a temperature profile approximated from the analytical solution of the heat transfer equation forced by ground heat flux. Temporally variable ground heat flux is estimated using non-gradient models when field observations are not available. Validation of the proposed model conducted against field data obtained from three Arctic forest and tundra sites demonstrates that the model is able to simulate both thaw depth and soil temperature profiles accurately. The model has the potential to estimate regional variability of the thaw depth for permafrost related applications.

Plain Language Summary The seasonally thawed layer on top of the permafrost (active layer) is a key component of the Arctic system affected by the strong warming trend over the past decades. This soil layer experiences a pronounced seasonal cycle of freezing and thawing processes caused by the availability of Sun's energy. Mathematical modeling of the thaw depth of the active layer has remained challenging. This study formulates a novel model for the simulation of the diurnal cycle of thawing process. The formulation is developed using innovative models of heat flux that goes into the soil and soil temperature profile. Ground heat flux is derived from available energy at the land surface using a theory of surface heat flux partition. The soil temperature profile is expressed using ground heat flux within the active layer. The proposed model has been validated against field observations during thawing season. The model simulation and field observations of the thaw depth are in a good agreement at three Arctic study sites with forest and tundra surface conditions. The proposed formulation can be used for modeling freeze-thaw cycles of the active layer at the regional scales since data on surface available energy can be obtained from remote sensing observations.

1. Introduction

The enhanced warming rates of the Arctic regions over the past decades (ACIA, 2004; Bekryaev et al., 2010; Chapin et al., 2005; Overpeck et al., 1997; Serreze et al., 2000) have stimulated active research on the permafrost dynamics (e.g., Jorgenson et al., 2006; Oelke et al., 2003; V. E. Romanovsky et al., 2010; Yi et al., 2018). There is a strong interest to further our understanding of the effect of increasing surface temperatures on the freeze-thaw cycles of the top layer in which water changes phase seasonally—referred to as the "active layer." Recent studies emphasize the modeling of the freeze-thaw cycles from the annual to sub-daily time scales (e.g., Bui et al., 2020; Evans & Ge, 2017; Riseborough et al., 2008; Walvoord & Kurylyk, 2016) for improving the understanding of the seasonality and variability of the active layer dynamics. Understanding of the freeze-thaw cycles is crucial for the livelihoods of communities who rely on the state of the ground for transportation or animal husbandry (Crate et al., 2017). This knowledge is also of utmost importance for understanding the dynamics of the biogeochemical processes in Arctic soils as seasonal swings to above freezing temperatures leads to the enhancement of decomposition rates of the accumulated carbon stocks (Schuur et al., 2015). The maximum thaw depth also informs engineering decisions related to infrastructure in the Arctic (Streletskiy et al., 2012).

ZHU ET AL. 1 of 13

Supervision: Jingfeng Wang, Valeriy Ivanov, Aleksey Sheshukov Validation: Modi Zhu Visualization: Modi Zhu Writing – original draft: Modi Zhu Writing – review & editing: Modi Zhu, Jingfeng Wang, Valeriy Ivanov, Aleksey Sheshukov While the freeze-thaw processes has been extensively studied (e.g., Miller, 1980), analytical treatment of the related heat transfer problems is limited. Analytical solutions of heat transfer equations for porous media under various initial and boundary conditions are well-developed for cases without water phase change (e.g., Carslaw et al., 1962; Crank, 1975). Developing analytical models of thaw depth has been challenging primarily due to the strong nonlinearity of the governing equation caused by the thaw front being a moving boundary of the study domain. Changing surface boundary conditions of temperature and heat flux further complicates the derivation of analytical solutions of the heat transfer equation.

Problems involving a moving freeze-thaw boundary are known as the Stefan problems (Vuik, 1993). The traditional models of freeze-thaw processes in porous media are formulated based on the two-phase (liquid and solid water) Stefan problem for the solution of the thaw depth with constant temperature boundary condition applied at the surface of a semi-infinite soil column (e.g., Alexiades & Solomons, 2018; Lunardini, 1981) (Appendix A). Common assumptions include (a) the temperature distribution of the liquid phase is described by a diffusion Equation A1, and (b) the temperature of the solid (ice) phase remains constant at the melting point (e.g., Lunardini, 1981). The rate of solid-to-liquid phase change at the thaw front equals to the conductive heat flux, known as the Stefan condition, is imposed as the boundary condition at the thaw front Equation A3.

The two-phase Stefan problem is strongly nonlinear due to the moving thaw front, whose location needs to be solved for. The analytical solution of temperature and thaw front location of the Stefan problem, referred to as the "Neumann similarity solution" or the "Neumann solution" Equations A4 and A5, predicts that the thaw front location is proportional to the square root of time since the onset of thaw process. Under certain conditions of the physical parameters (i.e., heat capacity of liquid water and latent heat of fusion), the Neumann solution becomes the Stefan solution (Lunardini, 1981) in which the thaw front location becomes a function of the constant surface temperature Equation A7. To our knowledge, an analytical solution of temperature and thaw front under changing surface temperature condition does not exist. Therefore, the existing analytical models of the thaw front based on the classical two-phase Stefan problem do not capture the effect of changing surface temperature and/or soil heat flux in reality on the thaw depth. A modified Stefan solution (Ladanyi & Andersland, 2004; Lunardini, 1981) for the estimation of thaw depth uses the degree-days thawing (DDT) index (Van Everdingen, 1998). The modified Stefan solution has been shown to outperform the classical solution in modeling freeze-thaw cycles at the annual scale (e.g., K. M. Hinkel & Nicholas, 1995; Nelson et al., 1997). However, it does not accurately simulate thaw depth at sub-daily time scales, which will deepen our understanding of the dynamics of the active layer, due to the neglect of soil surface energy balance and time-varying soil properties such as thermal conductivity and diffusivity (K. M. Hinkel & Nicholas, 1995).

The semi-empirical solution of the Stefan problem at annual scale was proposed by assuming the sinusoidal seasonal variation of air temperature (Kudryavtsev et al., 1977). This semi-empirical solution was applied to estimating thaw depth in the coastal region of Alaska (V. Romanovsky & Osterkamp, 1997). It was found that thaw depth depends not only on the thawing index defined as the cumulative number of degree-days above zero degree Celsius for a given time, but also on the time history of surface temperature. Further application of the semi-empirical solution to freeze-thaw cycles for the northern hemisphere (Anisimov et al., 1997) suggests that the semi-empirical model is not well constrained by surface energy balance. The modified Stefan solution in terms of the thawing index has been used to describe freeze-thaw cycles in the Arctic region in the coupled land-atmosphere models such as SiB2 (X. Li & Koike, 2003; Sellers et al., 1996), SHAW (Flerchinger, 2000), CLM (Oleson et al., 2013), and CAS-FGOALS-g3 (L. Li et al., 2020; R. Li et al., 2021). It was found that the modified Stefan solution does not close the energy budget of the thaw process. For example, the modified Stefan solution using thawing index in CLM over-estimates freeze/thaw depth due to ignoring soil conductive heat flux (e.g., Gao et al., 2019).

The objective of this study is to formulate an analytical model of thaw depth under changing ground heat flux at sub-daily to seasonal time scale.

2. Model Formulation

The conservation of energy for the active layer is expressed as,

ZHU ET AL. 2 of 13

1698996, 2024, 5, Downloaded from https://agupubs.onlinelibrary.wiley.com/doi/10.1029/2023JD039453, Wiley Online Library on [19/12/2024]. See the Terms and o

$$\int_0^{S(t)} C_s [T(x,t) - T_m] dx + \lambda_f \rho_i \int_0^{S(t)} \theta_i(x) dx = \int_0^t G(\tau) d\tau \tag{1}$$

where S(t) (m) is the thaw depth at time t, T(x,t) (°C) the soil temperature at depth x, G (Wm⁻²) the ground heat flux (i.e., the conductive heat flux at the surface of the mineral soil layer), $\theta_i(x)$ the pre-thawing ice content and τ the integration (dummy) time variable. The parameters include bulk soil volumetric heat capacity C_s , density of ice ρ_i (kgm⁻³), latent heat of fusion λ_f (3.34 × 10⁵ Jkg⁻¹), and the melting-point of water T_m (0°C). Thawing starts when the active layer reaches isothermal condition at T_m (e.g., Frauenfeld et al., 2007; Outcalt et al., 1990). The first integral on the left-hand side represents the thermal energy storage from the surface down to the thaw front, and the second term is the latent heat of fusion of ice. The integral on the right-hand side is the energy supply for ice melting and heat storage change provided by ground heat flux into the mineral soil layer. The frozen active layer beyond thaw front is not included in Equation 1 until thaw front reaches the certain depth.

An analytical solution of T(x, t) for a one-dimensional semi-infinite domain (Carslaw et al., 1962) without phase change is,

$$T(x,t) = T_0 + \frac{1}{I_s\sqrt{\pi}} \int_0^t \exp\left[-\frac{x^2}{4\alpha_s(t-\tau)}\right] \frac{G(\tau)d\tau}{\sqrt{t-\tau}}$$
 (2)

where I_s is the bulk soil thermal inertia (Jm⁻²K⁻¹s^{-1/2}), α_s the bulk soil thermal diffusivity (m²s⁻¹), and T_0 the initial soil temperature assumed to be uniform with depth (taken as T_m in this study). For the case of ice melting, the temperature profile during the thawing period can be approximated by T(x, t) - T(S(t), t) when liquid-solid water interface moves slowly (Mamode, 2013). Thaw front temperature remaining at T_m requires $T(S(t), t) = T_m$. Substituting Equation 2 into Equation 1 leads to a nonlinear integral equation of S(t) (Appendix B),

$$\lambda_f \rho_i \int_0^{S(t)} \theta_i(x) dx = \int_0^t G(\tau) \left[erfc \left(\frac{S(\tau)}{2\sqrt{\alpha_s(t-\tau)}} \right) + \frac{S(\tau)}{\sqrt{\alpha_s \pi(t-\tau)}} \exp \left(-\frac{S^2(\tau)}{4\alpha_s(t-\tau)} \right) \right] d\tau \tag{3}$$

where erfc is the complementary error function, and the integration lower limit $\tau = 0$ is the time when the land surface starts to thaw.

G in Equations 1–3 is ground heat flux at the surface of mineral soil experiencing freeze-thaw cycles. When field observation of G is not available, G can be estimated from the conductive heat flux Q at the surface of peat layer, that is, a partially decomposed organic material on the top of mineral soil (Robinson et al., 2003), using the maximum entropy production (MEP) model (J. Wang & Bras, 2011), which has been successfully applied to modeling the surface energy budget for the Arctic permafrost regions (El Sharif et al., 2019),

$$Q = R_n - E - H$$

$$R_n = \left[1 + B(\sigma) + \frac{B(\sigma)}{\sigma} \frac{I_s}{I_0 |H|^{\frac{1}{6}}} \right] H$$

$$E = B(\sigma)H$$

$$B(\sigma) = 6 \left(\sqrt{1 + \frac{11}{36}\sigma} - 1 \right), \ \sigma \equiv \frac{\lambda^2}{c_p R_v} \frac{q_s}{T_s^2}$$

$$(4)$$

where E (Wm $^{-2}$) and H (Wm $^{-2}$) are latent and sensible heat flux respectively, R_n (Wm $^{-2}$) the net radiative flux, T_s (K) the soil surface temperature, q_s the surface specific humidity, I_s (Jm $^{-2}$ K $^{-1}$ s $^{-1/2}$) the soil thermal inertia, I_0 the "apparent thermal inertia of the air" (J. Wang & Bras, 2009), λ (2.5 × 10 6 Jkg $^{-1}$) the latent heat of vapourization of liquid water, c_p (10 3 Jkg $^{-1}$ K $^{-1}$) the specific heat of the air at constant pressure, and R_v (461 Jkg $^{-1}$ K $^{-1}$) the gas constant of water vapor. Net radiation toward the land surface is conventionally defined as positive and the signs of Q, E, and H are opposite to that of net radiation. The good performance of the MEP model for the simulation of surface soil heat flux over tundra peat layer, a special type of "organic soil" characterized by low thermal inertia

ZHU ET AL. 3 of 13

.com/doi/10.1029/2023JD039453, Wiley Online Library on [19/12/2024]. See the Terms

Table 1 The Volumetric Ice Content Profile $\theta_i(x)$ Measured at the Three Sites Prior to the Thaw Period

		Sites	
Depth (cm)	T1	T2	TR
6	0.10	0.20	0.33
20	0.15	0.16	0.30
40	0.15	0.20	0.23
70	0.16	0.08	0.25
100	NA	0.13	0.32

Note. "NA" for site T1 indicates that ice was not present at the depth of 100 cm at this site

than the mineral soils due to low density and thermal conductivity, has been reported (El Sharif et al., 2019). G in Equations 1–3 is expressed in terms of Q (Z.-H. Wang & Bou-Zeid, 2012; Yang & Wang, 2014),

$$G(t) = \int_0^t erfc \left[\frac{D}{2\sqrt{\alpha_t(t-\tau)}} \right] dQ(\tau)$$
 (5)

where D is the depth of the peat layer (m), α_t the thermal diffusivity of the bulk peat layer material (m² s⁻¹), and $\tau = 0$ is the same starting time as that in Equation 3.

3. Study Sites and Field Data

Soil temperature, soil heat flux, and other meteorological variables were collected in 2019 at a moss-lichen tundra site (66°53.652′N, 66°45.881′E)

and two larch forest sites (66°53.923'N, 66°45.442'E; 66°53.760'N, 66°45.623'E) on the eastern slope of Polar Urals, Yamal-Nenets Autonomous District, Russia (Ivanov et al., 2018). The three sites (labeled as "TR (tundra)," "T (trees)1," and "T (trees)2") are located in an Arctic tundra-forest transitional zone along the boundary of discontinuous permafrost region (Obu et al., 2019). The mean frost-free period is 94 days and the growing season from mid-June to mid-August. The mean annual precipitation is 500-600 mm with about 50% in the form of snow and sleet. Moss-lichen tundra with rock outcrops and deciduous shrub communities are the dominant land covers. Two "Trees" sites are covered with mountain heath tundra encroached by the Siberian larch in the past 30 years. The current surface canopy covers are 50% (Trees 1) and 30% (Trees 2), 7-8 m average height, and individual trees reaching 10 m. Sensors are identical at all sites for measuring soil temperature at five depths (6, 20, 40, 70, 100 cm). Surface temperature was measured using infrared radiometers (SI-111; Apogee Instruments, Inc., Logan, Utah, USA). Net radiation and shortwave radiation (single-channel NR Lite2 Net Radiometer and CMP 3 Pyranometer; Kipp and Zonen, Delft, Netherlands) were measured at 8 m ("Tundra") and 13.5 m ("Trees") height. Soil heat fluxes were measured by soil heat flux plate (HFP01; HuksefluxUSA, Inc., Center Moriches, NY, USA) buried at 6 cm depth into mineral soil with a peat layer of varying thickness: 8 cm at TR, 5 cm at T1, and 6 cm at T2. Soil water content and temperature were measured using multivariable time differential reflectometer (TDR) sensors (CS655; Campbell Scientific, Inc., Logan, Utah, USA). All soil and meteorological variables are sampled at 30 min interval.

The observed thaw depths are identified by the abrupt changes in liquid water content and soil temperature (Patterson & Smith, 1981). The active-layer thaw process is strongly affected by the ice content (Brown et al., 2000). When field data of soil ice content do not exist, pre-thawing ice content $\theta_i(x)$ (Table 1) is estimated from the difference of pre- and post-thawing soil liquid water content (Overduin & Kane, 2006). Depth dependence of $\theta_i(x)$ caused by soil moisture distribution at the onset of seasonal freezing affects the water content-dependent model parameters including thermal diffusivity α_s and thermal inertia I_s (K. M. Hinkel & Nicholas, 1995; Ochsner & Baker, 2008). An estimation of thermal diffusivity is provided in Appendix C.

4. Results

The thaw depth model in Equation 3 is validated by comparing the modeled thaw depth and temperature profile with the field observations at the three sites.

4.1. Model Simulations of Thaw Depth

Ground heat flux G obtained from Equation 5 is in good agreement with the soil heat flux measured at 6 cm below the mineral soil surface shown in Figure 1 with the corresponding statistics in Table 2. The accurate estimation of G provides reliable input for the proposed model of thaw depth. The corresponding soil heat flux estimated under the condition of the Stefan solution Equation A8 is also shown in Figure 1. The Stefan model substantially overestimates G at the beginning of thawing and underestimates G in later stages, suggesting a substantial bias in the energy budget of the Stefan model. The effect of the energy budget imbalance on the thaw depth in the classical solution is discussed in detail below.

ZHU ET AL. 4 of 13

21698996, 2024, 5, Downloaded from https://agupubs.onlinelibrary.wiley.com/doi/10.1029/2023ID039453, Wiley Online Library on [19/12/2024]. See the Terms and Conditions (https://onlinelibrary.wiley.com/terms

and-conditions) on Wiley Online Library for rules of use; OA articles are governed by the applicable Creative Commons License

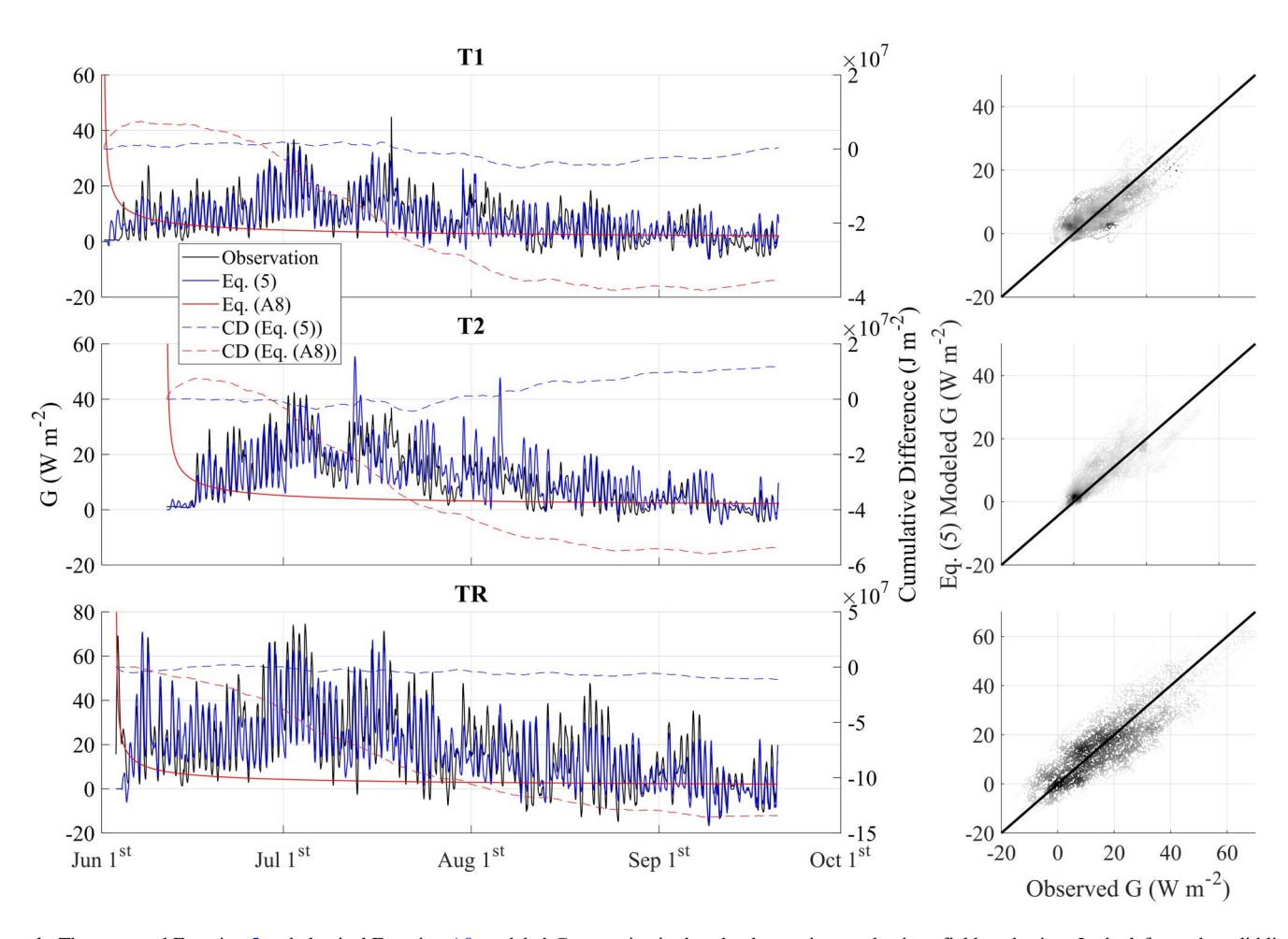


Figure 1. The proposed Equation 5 and classical Equation A8 modeled *G* versus in-situ hourly observations at the three field study sites. In the left panels, solid lines represent *G* values, dashed lines represent cumulative differences (CD), that is, cumulative modeled *G*—cumulative observed *G*.

The modeled thaw depth S(t) at the study sites is shown in Figure 2. At T1 site, water content at 70 and 100 cm are observed to change almost simultaneously, indicating that the soil beyond 70 cm was not fully frozen during the pre-thawing season. It implies that the maximum depth of freezing at the T1 site is 70 cm. The occurrence of an unfrozen layer is possibly due to the isolated talik (Lunardini, 1981), which remained unfrozen during the winter season. At the T2 site, thawing starts on June 11th and the active layer thickness is larger than 1 m (the maximum monitoring depth). Thawing starts on May 31st and June 3rd at T1 and TR site, respectively.

Table 2Statistics of the Modeled ("Model") Soil Heat Flux Compared to Half-Hourly Observations ("OBS")

		Model			
Sites	Mean OBS (Wm ⁻²)	Mean (Wm ⁻²)	R	RMSE (Wm ⁻²)	NSE
T1	7.89	7.94	0.80	4.63	0.64
T2	10.5	11.9	0.80	6.21	0.58
TR	18.50	17.33	0.83	9.68	0.68

Note. R is correlation coefficient; RMSE is the root mean square error; NSE is the Nash Sutcliffe Efficiency.

Figure 2 shows that both the observed and simulated thaw depths do not necessarily follow the square root of time function according to the Stefan solution in Equation A7. The thawing rates at all sites accelerate during the period from mid-June to early July corresponding to higher soil heat flux (Figure 1). The increasing thawing rates in the middle of the thawing season are also likely to be attributed to relatively low ice content (e.g., Table 1, T2: 40–70 cm; TR: 20 to 40 cm).

This comparison analysis highlights the crucial role of ground heat flux in modeling thaw depth at sub-seasonal time scales. As compared to the Stefan solution based models, the proposed model yields improved simulation of thaw depth forced by changing ground heat flux. Equation 3 simulates S(t) more accurately than the classical Stefan solution Equation A7 and the modified Stefan solution Equation A9 (Figure 2). The two Stefan solution-based models overestimate the thaw depth during the early stage of

ZHU ET AL. 5 of 13

21698996, 2024, 5, Downloaded from https://agupub.s. onlinelibrary.viley.com/doi/10.1029/2023JD099433, Wiley Online Library on [19/1/20204]. See the Terms and Conditions (https://onlinelibrary.viley.com/terms-and-conditions) on Wiley Online Library for rules of use; OA articles are governed by the applicable Creative Commons Licensia

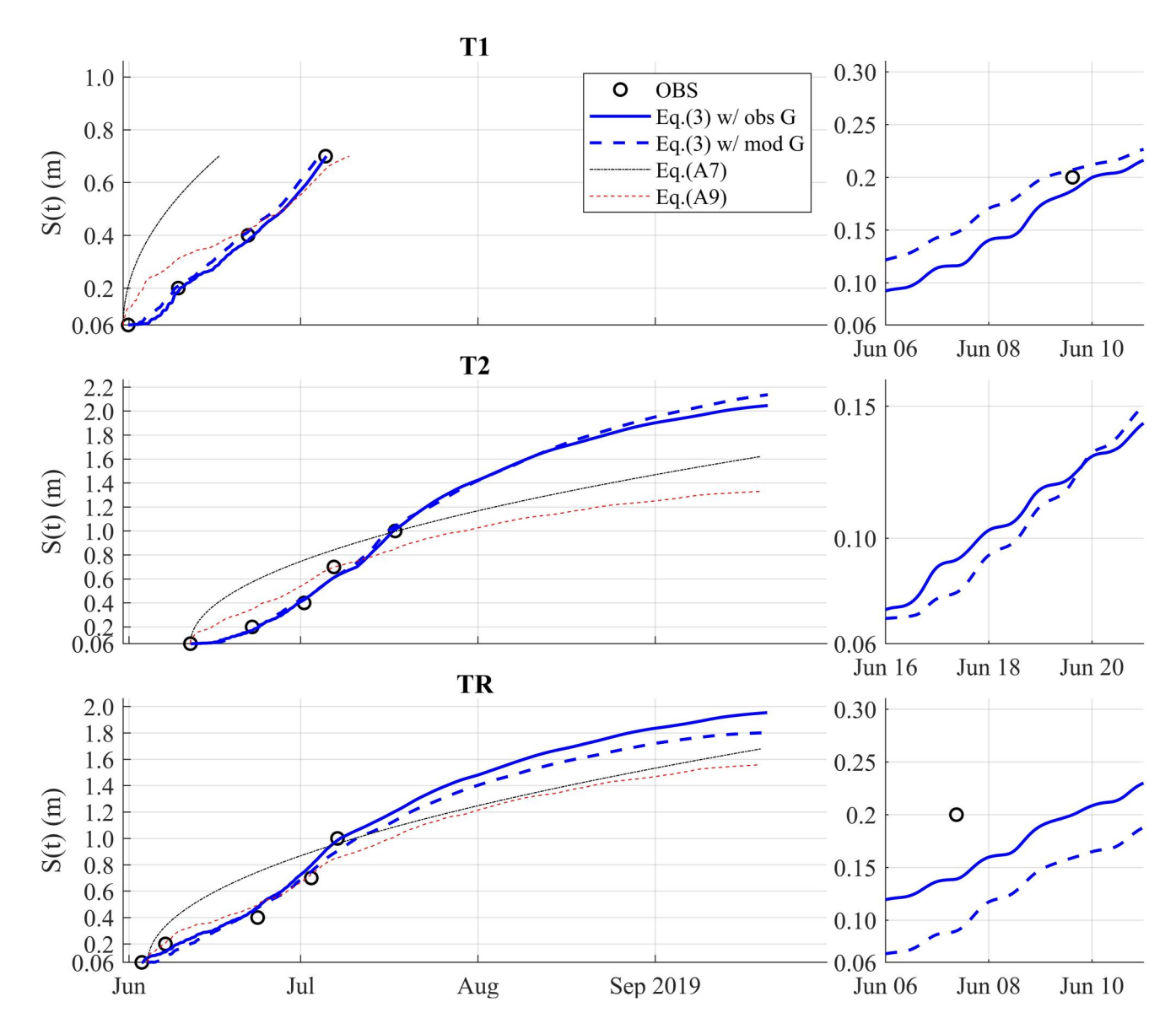


Figure 2. The observed thaw depth ("OBS") versus the two classical solution based models (Equation A7 and Equation A9), and the proposed model (Equation 3) with the MEP modeled ground heat flux ("w/mod G") and observed ground heat flux ("w/obs G") at the field study sites. The soil parameters remain unchanged below 1 m (the maximum measurement depth). $\kappa_L = 0.12 \text{ W m}^{-1} \text{ K}^{-1}$ in Equation A7 and $T_s = 0.39$ °C the mean observed surface temperature of the thawing season. The right panels show a detailed view of diurnal behaviors of the proposed model.

thawing. The biases of the Stefan solution-based models are arguably caused by the biases of ground heat flux input (Figure 1). The discontinuous surface temperature boundary condition in the Stefan solution Equation A7 implies infinite initial ground heat flux, leading to the overestimation of thaw depth during the early stage of thawing. The steady-state surface temperature during the later stage of thawing leads to underestimated ground heat flux and hence the thaw depth. The temperature-day model in Equation A9 using a more realistic surface temperature boundary condition outperforms Equation A7 with the steady-state boundary condition of surface temperature. The modified Stefan solution does not in general close the surface energy budget caused by inaccurate representation of ground heat flux input.

As shown in Figure 2, the results from the proposed model yield estimation of the annual active layer depth: 2.04 m for T2 and 1.95 m for TR, based on observed ground heat flux, and 2.13 m at T2 and 1.80 m at TR, derived from non-gradient methods modeled ground heat flux.

ZHU ET AL. 6 of 13

21698996, 2024, 5, Downloaded from https://agupubs.onlinelibrary.wiley.com/doi/10.1029/2023JD039453, Wiley Online Library on [19/12/2024]. See the Terms

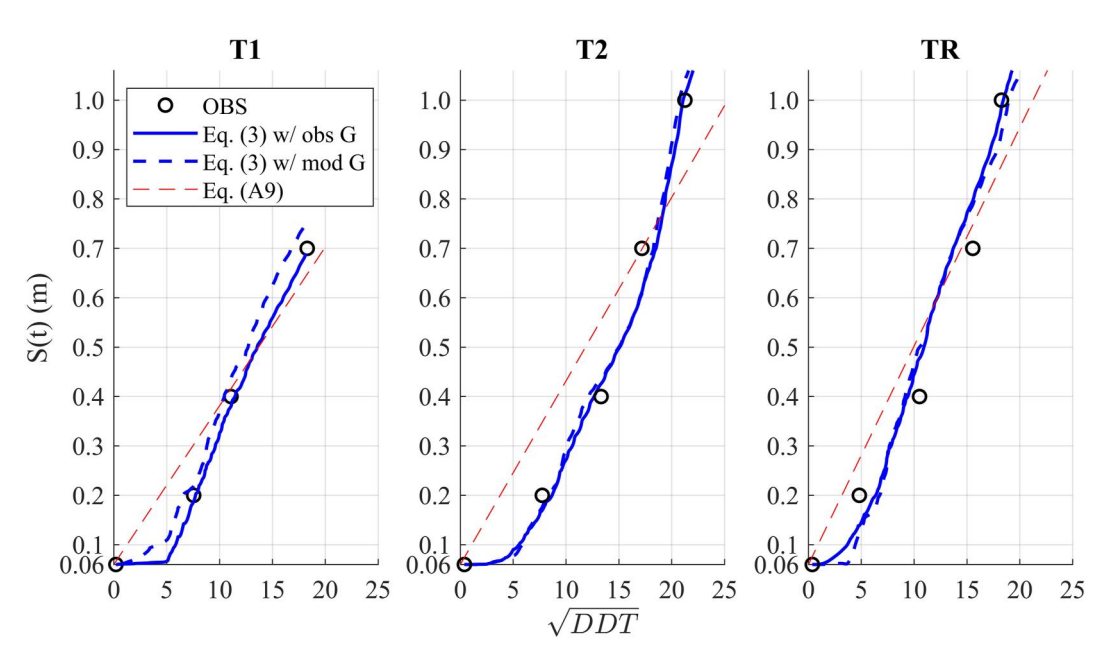


Figure 3. Modeled and observed S(t) versus DDT^{1/2} at the study sites.

S(t) estimated using Equation A9 has evident biases compared to S(t) using Equation 3 and observations (Figures 2 and 3). The thaw depth is underestimated when the thawing index is low. Due to the "zero-curtain" effect, that is, temperatures remain near 0°C over extended periods in freezing or thawing soils (Outcalt et al., 1990), the soil temperature of the top layer remains close to the melting point during the early stage of thawing associated with nearly zero ground heat flux. The thawing index however is calculated using the cumulative air temperature, which yields a higher ground heat flux than what is implied by the nearly isothermal state of the top soil. The estimated constant b in Equation A9 is arguably partially responsible for the biases of the S(t) solution based on the thawing index (K. M. Hinkel & Nicholas, 1995). Specifically, the coefficient b in Equation A9 estimated using temporally aggregated dynamics of the thaw process does not represent the effect of temporally and spatially varying ice content and soil thermal properties on the thawing rate.

4.2. Approximate Analytical Solution of Soil Temperature Profile

The modeled and observed soil temperature profiles are shown in Figure 4a-4c. The modeled and observed soil temperature are in good agreement with maximum modeling errors less than 3°C. The soil temperature remaining at around 0°C suggests that the thaw front has not reached the corresponding depth, supporting the assumption of isothermal temperature profile before thawing starts. Meanwhile, the observed soil temperature at the T2 site started to increase on Jun 13th before the thaw front reaches 20 cm on Jun 24th (Figure 4b), which is inconsistent with the water content measurement. This discrepancy is likely caused by the vertical flow of liquid water creating additional advective heat source not accounted in the proposed model. That explains the under-estimation of soil temperature during the first 20 days. The presence of a talik layer at the T1 site significantly alters the thermodynamics at the thaw front evidenced by the thaw front reaching 70 cm depth on July 5th (Figure 4a). When talik is present, the thermal energy at the thaw front is entirely used for changing soil temperature, rather than melting ice. Equation 3, which holds under the condition that the thermal energy provided by G is used for both ice melt and soil temperature change, does not describe the thaw front dynamics. The statistics of the observed and modeled soil temperature is shown in Table 3. The proposed model effectively estimates soil temperature profile with R higher than 0.68 (mostly higher than 0.9) and RMSE $\leq 1.73^{\circ}$ C (mostly lower than 1°C). As compared to the observed ground heat flux G, Equation 3 using the MEP modeled G simulates soil temperature profile in closer agreement with the observations. This finding confirms the critical role of changing ground heat flux in the thawing process and supports the use of the MEP model in the simulation of surface energy budget over the Arctic permafrost regions.

ZHU ET AL. 7 of 13

21698996, 2024, 5, Downloaded from https://agupubs.onlinelibrary.wiley.com/doi/10.1029/2023JD039453, Wiley Online Library on [19/12/2024]. See the Terms and Conditional Condi

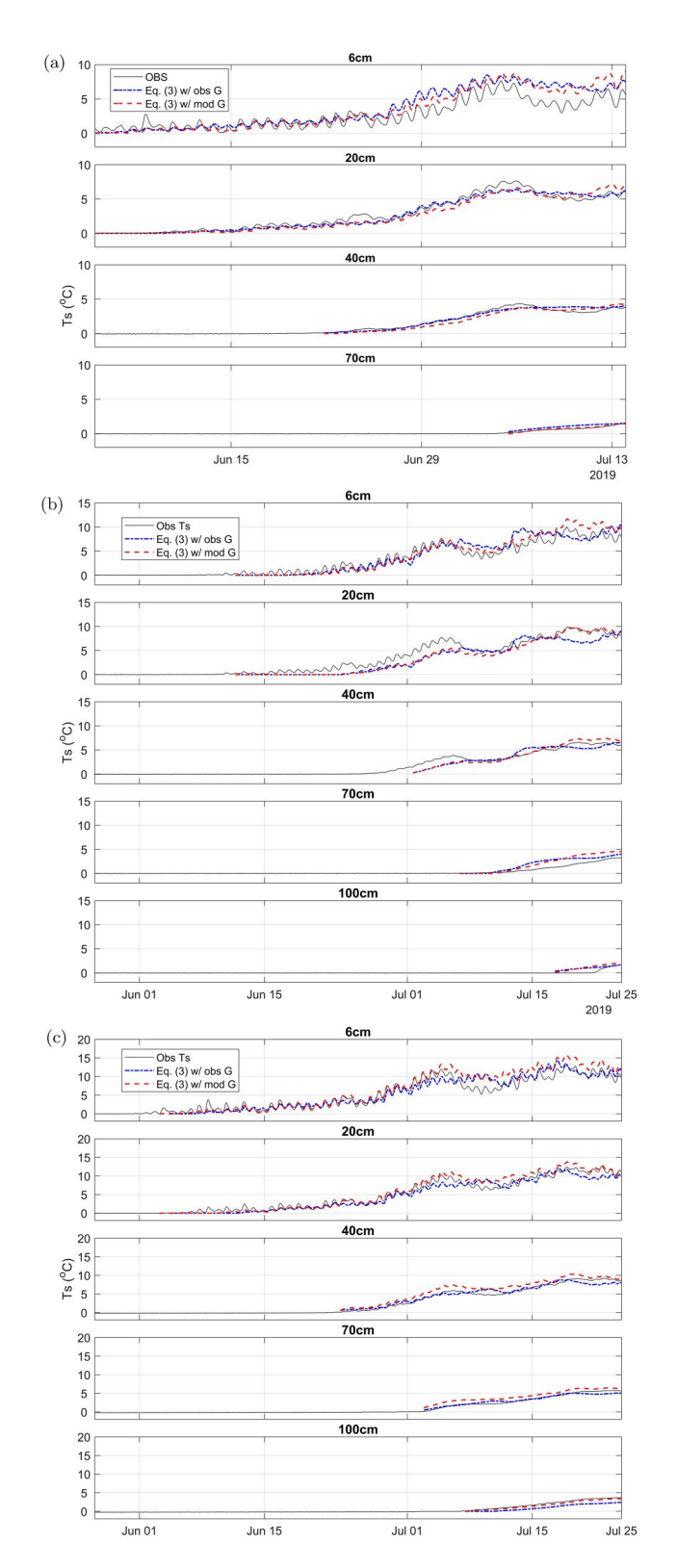


Figure 4. Modeled versus observed soil temperature. Soil depth is indicated in the subplot titles. (a) Modeled versus observed hourly soil temperature at T1 site (5 Jun 2019 to 13 July 2019). (b) Modeled versus observed hourly soil temperature series at T2 site (27 May 2019 to 25 July 2019). (c) Modeled versus observed hourly soil temperature at TR site (27 May 2019 to 25 July 2019).

5. Discussion

The behavior of the permafrost active layer thawing can be described by the two-phase Stefan problem. The governing equation of the two-phase Stefan problem is highly nonlinear due to the moving thaw front. Traditional models of thaw depth have been formulated at seasonal scale. While recent studies have highlighted the need to refine modeling to shorter time scales, aiming at enhancing the understanding of the seasonality and variability of the active layer dynamics. The semi-empirical temperature-day model of thaw depth cannot resolve diurnal cycle of thaw depth and does not close the energy balance.

As discussed in Section 2, a pivotal assumption in the proposed model development involves refining the temperature profile at the thaw depth. This refinement, grounded in a no phase change temperature profile, introduces minimal deviations in modeling the soil temperature profile while leading to the satisfaction of Earth's surface energy budget. The results demonstrate that the trade-off is minimal, yet the benefits in terms of model accuracy and representation of energy dynamics are substantial.

Additionally, the model's robustness extends beyond the thawing phase; it theoretically applies to the freezing phase as well, traditionally viewed as the antithesis of thawing. A key distinction in modeling the freezing phase, particularly in Arctic regions, is the presence of snow cover, which significantly reduces the magnitude of soil heat flux. Incorporating snow coverage into the model is essential to reflect the actual thermal conditions during the freezing process.

Data from field experiments in the Polar Ural Mountains includes variables like ground surface heat flux, soil temperature, and soil moisture content, etc. A significant constraint, however, lies in the absence of direct ice content readings. This research currently infers ice content from the differences in soil liquid water content before and after thawing events. Accurate ice content data would improve the modeling accuracy given its critical role in the active layer's thermodynamics and justify an application of the proposed models for the simulation of thaw depth at the regional scales—a topic of follow-up studies.

6. Conclusions

The proposed analytical model of thaw depth forced by changing ground heat flux improves the simulation of the diurnal cycle of the thaw depth of the permafrost active layer. Conductive heat flux at the surface of peat canopy can be calculated from net radiation using the MEP model of surface heat fluxes. Ground heat flux at the surface of mineral soil layer can be estimated using an approximate analytical solution of heat conduction in the peat layer. The validation analysis of the model against field observations of soil temperature and moisture at the Arctic permafrost region covered with forest and tundra canopy confirms its performance. The abundance of remote sensing data of net radiation may facilitate its application to modeling freeze-thaw cycle of permafrost active layer at regional scale.

ZHU ET AL. 8 of 13

21698996, 2024, 5, Downloaded from https://agupubs.onlinelibrary.wiley.com/doi/10.1029/2023JD039453, Wiley Online Library on [19/12/2024]. See the Terms and Conditions

Table 3
The Correlation Coefficient (R) and Root Mean Square Error (RMSE) of Modeled Hourly Soil Temperature Series

			T1	T2		TR	
Site depth		R	RMSE (°C)	R	RMSE (°C)	R	RMSE (°C)
6 cm	w/Obs G	0.87	1.50	0.88	1.25	0.90	1.36
	w/Mod G	0.92	1.32	0.97	1.08	0.97	1.73
20 cm	w/Obs G	0.96	0.50	0.90	1.44	0.95	1.01
	w/Mod G	0.96	0.61	0.94	1.20	0.99	0.92
40 cm	w/Obs G	0.94	0.35	0.78	0.93	0.95	0.70
	w/Mod G	0.94	0.44	0.96	0.87	0.98	1.23
70 cm	w/Obs G	0.88	0.34	0.82	0.99	0.96	0.44
	w/Mod G	0.97	0.08	0.95	1.13	0.99	1.02
100 cm	w/Obs G		NA	0.74	0.68	0.98	1.03
	w/Mod G			0.68	0.82	0.99	0.31

Note. "w/Obs G" are calculated by using soil heat flux observed in Equation 3; "w/Mod G" are calculated by using soil heat flux modeled in Equation 3. "NA" for T1 site indicates that ice was not present at the depth of 100 cm at T1 site.

Appendix A: Two-Phase Stefan Problem, Neumann Similarity Solution, and Modified Stefan Solution

The classical Neumann solution of the two-phase Stefan problem for the process of thaw can be represented by the heat conduction equation for a one-dimensional semi-infinite medium (e.g., water) with a moving thaw front S(t) (e.g., Alexiades & Solomons, 2018),

$$\frac{\partial T(x,t)}{\partial t} = \alpha_L \frac{\partial^2 T(x,t)}{\partial x^2}, \ 0 \le x \le S(t)$$

$$T(x,t) = T_m, \ S(t) \le x < \infty, t \ge 0$$
(A1)

where S(t) is the thaw depth, T(x, t) is the temperature profile at time t, x is the location coordinate with the surface at x = 0, $T_m(0^{\circ}\text{C})$ is the thawing temperature, and α_L is the thermal diffusivity (m²s⁻¹) of liquid medium subject to the initial and boundary conditions

$$T(x,0) = T_m$$

 $T(0,t) = T_s > T_m, t > 0$ (A2)

where T_s is the surface temperature, which is assumed to be constant. The Stefan condition at the moving boundary, which states that the rate of energy arriving at the front by heat conduction is equal to the rate of heat absorbed by the ice in the soil as its heat of melting, is represented by

$$\rho_s \lambda_f \frac{dS(t)}{dt} = -\kappa_L \frac{\partial T(S(t), t)}{\partial x}$$

$$S(0) = 0$$
(A3)

where κ_L is the thermal conductivity of liquid medium, ρ_s is the density of solid medium, and λ_f is the latent heat of fusion. The Neumann similarity solution is given as

$$T(x,t) = T_s - (T_s - T_m) \frac{erf\left(\frac{x}{2\sqrt{\alpha_L t}}\right)}{erf(\gamma)}$$

$$S(t) = 2\gamma\sqrt{\alpha_L t}$$
(A4)

ZHU ET AL. 9 of 13

21698996, 2024, 5, Downloaded from https://agupubs.onlinelibrary.wiley.com/doi/10.1029/2023JD039453, Wiley Online Library on [19/12/2024]. See the Terms and Conditions

where erf is the error function and γ is the solution of the transcendental equation:

$$\frac{\exp(-\gamma^2)}{\operatorname{erf}(\gamma)} = \sqrt{\pi} \gamma \frac{\lambda_f}{C_L(T_s - T_m)} \tag{A5}$$

where C_L is the heat capacity of the liquid medium. For small γ , Equation A5 reduces to (e.g., Lunardini, 1981),

$$\gamma = \sqrt{\frac{C_L(T_s - T_m)}{2\lambda_f}} \tag{A6}$$

leading to the "Stefan solution,"

$$S(t) = \sqrt{\frac{2\kappa_L(T_s - T_m)}{\lambda_f \rho_s}} t \tag{A7}$$

The corresponding ground heat flux is expressed as,

$$G = \frac{k(T_s - T_m)}{\sqrt{\pi \alpha_L} erf(\gamma)} \frac{1}{\sqrt{t}}$$
(A8)

A modified Stefan solution of thaw depth is expressed in terms of *DDT* (°C day), the cumulative number of degree-days above zero degree Celsius since the onset of thawing (K. M. Hinkel & Nicholas, 1995),

$$S(t) = b\sqrt{DDT} \equiv b\sqrt{\int_0^t \left[T_s(\tau) - T_m\right] d\tau}, T_s > T_m$$
(A9)

where $b \text{ (m}^{\circ}\text{C}^{-1/2} \text{ day}^{-1/2})$ is assumed to be a constant fitting parameter, calculated from the best-fit line to the observations.

Appendix B: Derivation of Equation 3

Based on Equation 2, T(S(t), t) can be expressed as:

$$T(S(t),t) = T_0 + \frac{1}{I_s\sqrt{\pi}} \int_0^t \exp\left(-\frac{S^2}{4\alpha_s(t-\tau)}\right) \frac{G(\tau)}{\sqrt{t-\tau}} d\tau$$
 (B1)

T(S(t)) is then considered as the temperature correction term to keep thaw front temperature remain at melting point. Applying the temperature correction term in the energy conservation equation 1 leads to

$$\int_{0}^{t} G(\tau)d\tau = \int_{0}^{S(t)} C_{s} \left[\frac{1}{I_{s}\sqrt{\pi}} \left[\int_{0}^{t} \exp\left(-\frac{x^{2}}{4\alpha_{s}(t-\tau)}\right) \frac{G(\tau)}{\sqrt{t-\tau}} d\tau - \int_{0}^{t} \exp\left(-\frac{S^{2}}{4\alpha_{s}(t-\tau)}\right) \frac{G(\tau)}{\sqrt{t-\tau}} d\tau \right] \right]$$

$$dx + \lambda_{f} \rho_{i} \int_{0}^{S(t)} \theta_{i}(x) dx$$
(B2)

As $I_s = C_s \sqrt{\alpha_s}$, Equation B2 can be expressed as

$$\int_{0}^{t} G(\tau) d\tau = \int_{0}^{S(t)} \left[\frac{1}{\sqrt{\alpha_{s}\pi}} \left[\int_{0}^{t} \exp\left(-\frac{x^{2}}{4\alpha_{s}(t-\tau)}\right) \frac{G(\tau)}{\sqrt{t-\tau}} d\tau \right] \right] dx + \lambda_{f} \rho_{i} \int_{0}^{S(t)} \theta_{i}(x) dx \\
- \int_{0}^{S(t)} \left[\frac{1}{\sqrt{\alpha_{s}\pi}} \left[\int_{0}^{t} \exp\left(-\frac{S^{2}}{4\alpha_{s}(t-\tau)}\right) \frac{G(\tau)}{\sqrt{t-\tau}} d\tau \right] \right] dx$$
(B3)

ZHU ET AL. 10 of 13

Equation B3 can be simplified by moving the first term on the right hand side to left hand side

$$\int_{0}^{t} erfc\left(\frac{S}{2\sqrt{\alpha_{s}(t-\tau)}}\right) G(\tau)d\tau = \lambda_{f}\rho_{i} \int_{0}^{S(t)} \theta_{i}(x)dx$$

$$-\int_{0}^{S(t)} \left[\frac{1}{\sqrt{\alpha_{s}\pi}} \left[\int_{0}^{t} \exp\left(-\frac{S^{2}}{4\alpha_{s}(t-\tau)}\right) \frac{G(\tau)}{\sqrt{(t-\tau)}} d\tau\right]\right] dx$$
(B4)

The second term on the right hand side in Equation B4 can be simplified through interchange of the order of integration and we can finally get the expression for the proposed model

$$\int_{0}^{t} G(\tau) \left[erfc \left(\frac{S(\tau)}{2\sqrt{\alpha_{s}(t-\tau)}} \right) + \frac{S(\tau)}{\sqrt{\alpha_{s}\pi(t-\tau)}} \exp\left(-\frac{S^{2}(\tau)}{4\alpha_{s}(t-\tau)} \right) \right] d\tau = \lambda_{f} \rho_{i} \int_{0}^{S(t)} \theta_{i}(x) dx$$
 (B5)

Equation B5 is the proposed equation. It is an implicit nonlinear integral equation that must be solved numerically.

Appendix C: Estimation of Thermal Diffusivity

In this research, thermal diffusivity α_s is estimated by numerically solving the inverse problem (e.g., K. Hinkel et al., 2001; McGaw et al., 1978; Nelson et al., 1985) of one-dimensional heat diffusion equation:

$$\frac{\partial T}{\partial t} = \alpha_s \frac{\partial^2 T}{\partial x^2} \tag{C1}$$

The time derivative can be approximated as:

$$\frac{\partial T}{\partial t} = \frac{T_i^{j+1} - T_i^{j-1}}{2\Delta t} \tag{C2}$$

And the space derivative can be approximated as:

$$\frac{\partial^2 T}{\partial x^2} = \frac{T_i^{j-1} - 2T_i^j + T_i^{j+1}}{\Delta x^2}$$
 (C3)

.com/doi/10.1029/2023/D039433, Wiley Online Library on [19/12/2024]. See the Terms and Conditions (https://onlinelibrary.wiley.com/terms-and-conditions) on Wiley Online Library for rules of use; OA articles are governed by the applicable Creative Commons License

where Δt and Δx are time and space resolutions, taken as 1 hr and 0.2 m respectively. The three layers of soil temperature are observed at the soil surface, 20 cm, and 40 cm. The inversely estimated diffusivities α_s at the three studied sites are summarized in Table C1.

Table C1Thermal Diffusivity α_s (mm² s⁻¹) at the Three Field Sites

		Sites	
Period	T1	T2	TR
~June 24th	0.94	1.82	1.62
June 24th ∼ August 9th	0.56	0.85	1.18
August 9th~	0.69	0.93	1.20

ZHU ET AL. 11 of 13

21698996, 2024, 5, Downloaded from https://agupubs.onlinelibrary.wiley.com/doi/10.1029/2023JD039453, Wiley Online Library on [19/12/2024]. See the Terms and Conditions (https://agupubs.onlinelibrary.wiley.com/doi/10.1029/2023JD039453, Wiley Online Library on [19/12/2024]. See the Terms and Conditions (https://agupubs.onlinelibrary.wiley.com/doi/10.1029/2023JD039453, Wiley Online Library on [19/12/2024]. See the Terms and Conditions (https://agupubs.onlinelibrary.wiley.com/doi/10.1029/2023JD039453, Wiley Online Library on [19/12/2024]. See the Terms and Conditions (https://agupubs.onlinelibrary.wiley.com/doi/10.1029/2023JD039453, Wiley Online Library on [19/12/2024]. See the Terms and Conditions (https://agupubs.com/doi/10.1029/2023JD039453, Wiley.com/doi/10.1029/2023JD039453, Wiley.com/doi/10.1029/2023JD039453,

com/terms-and-conditions) on Wiley Online Library for rules of use; OA articles

are governed by the applicable Creative Commons Licensi

Data Availability Statement

All data sets for this research are available at the National Science Foundation Arctic Data Center (T1 site (Ivanov et al., 2023a), T2 site (Ivanov et al., 2023b), TR site (Ivanov et al., 2023c)).

Acknowledgments

This research is sponsored by the National Science Foundation (NSF) Office of Polar Programs Grants 1724633 and 2126797 (Georgia Tech), 1725654, 2139432, and 2126792 (University of Michigan) and 1724868 (Kansas State University), V. Ivanov and V. Mazepa acknowledge the support from project RUB1-7032-EK-11 funded by the U.S. Civilian Research & Development Foundation, V. Ivanov was also partly supported by the NSF Navigating the New Arctic Program Grant 1928014. V. Mazepa acknowledges the partial support from Grant RFBR-19-05-00756 from the Russian Foundation for Basic Research. All authors are extremely grateful for the generous support of data collection program by the Arctic Research Station, Plant and Animal Ecology Institute, the Russian Academy of Sciences, the Urals Branch, Russia. We wholeheartedly thank the staff of the station Yuriy Trubnikov, V. Osokin, G. Popov, and V. Shtro for their technical and logistical support and extensive fieldwork.

References

ACIA. (2004). Impacts of a warming Arctic—Arctic climate impact assessment. Cambridge University Press.

Alexiades, V., & Solomons, A. D. (2018). Mathematical modeling of melting and freezing processes. Routledge.

Anisimov, O. A., Shiklomanov, N. I., & Nelson, F. E. (1997). Global warming and active-layer thickness: Results from transient general circulation models. *Global and Planetary Change*, 15(3–4), 61–77. https://doi.org/10.1016/s0921-8181(97)00009-x

Bekryaev, R. V., Polyakov, I. V., & Alexeev, V. A. (2010). Role of polar amplification in long-term surface air temperature variations and modern arctic warming. *Journal of Climate*, 23(14), 3888–3906. https://doi.org/10.1175/2010jcli3297.1

Brown, J., Hinkel, K. M., & Nelson, F. (2000). The circumpolar active layer monitoring (CALM) program: Research designs and initial results. *Polar Geography*, 24(3), 166–258. https://doi.org/10.1080/10889370009377698

Bui, M. T., Lu, J., & Nie, L. (2020). A review of hydrological models applied in the permafrost-dominated arctic region. *Geosciences*, 10(10), 401. https://doi.org/10.3390/geosciences10100401

Carslaw, H. S., Jaeger, J. C., & Feshbach, H. (1962). Conduction of heat in solids. *Physics Today*, 15(11), 74–76. https://doi.org/10.1063/1.

Chapin, F. S., III., Sturm, M., Serreze, M. C., McFadden, J. P., Key, J. R., Lloyd, A. H., et al. (2005). Role of land-surface changes in arctic summer warming. *Science*, 310(5748), 657–660. https://doi.org/10.1126/science.1117368

Crank, J. (1975). The mathematics of diffusion. Oxford University Press.

Crate, S., Ulrich, M., Habeck, J. O., Desyatkin, A. R., Desyatkin, R. V., Fedorov, A. N., et al. (2017). Permafrost livelihoods: A transdisciplinary review and analysis of thermokarst-based systems of indigenous land use. *Anthropocene*, 18, 89–104. https://doi.org/10.1016/j.ancene.2017.

El Sharif, H., Zhou, W., Ivanov, V., Sheshukov, A., Mazepa, V., & Wang, J. (2019). Surface energy budgets of arctic tundra during growing season. *Journal of Geophysical Research: Atmospheres*, 124(13), 6999–7017. https://doi.org/10.1029/2019jd030650

Evans, S. G., & Ge, S. (2017). Contrasting hydrogeologic responses to warming in permafrost and seasonally frozen ground hillslopes. Geophysical Research Letters, 44(4), 1803–1813. https://doi.org/10.1002/2016gl072009

Flerchinger, G. N. (2000). The simultaneous heat and water (SHAW) model: Technical documentation. Northwest Watershed Research Center USDA Agricultural Research Service.

Frauenfeld, O. W., Zhang, T., & Mccreight, J. L. (2007). Northern hemisphere freezing/thawing index variations over the twentieth century. International Journal of Climatology, 27(1), 47–63. https://doi.org/10.1002/joc.1372

Gao, J., Xie, Z., Wang, A., Liu, S., Zeng, Y., Liu, B., et al. (2019). A new frozen soil parameterization including frost and thaw fronts in the community land model. *Journal of Advances in Modeling Earth Systems*, 11(3), 659–679. https://doi.org/10.1029/2018ms001399

Hinkel, K., Paetzold, F., Nelson, F., & Bockheim, J. (2001). Patterns of soil temperature and moisture in the active layer and upper permafrost at Barrow, Alaska: 1993–1999. *Global and Planetary Change*, 29(3–4), 293–309. https://doi.org/10.1016/s0921-8181(01)00096-0

Hinkel, K. M., & Nicholas, J. R. (1995). Active layer thaw rate at a boreal forest site in central Alaska, USA. Arctic and Alpine Research, 27(1), 72–80. https://doi.org/10.2307/1552069

Ivanov, V., Sheshukov, A., Wang, J., El Sharif, H., Liu, D., Mazepa, V., et al. (2018). Changes in surface processes due to tree expansion into tundra, Polar Urals, Russia. 2018 AGU Fall Meeting, #A531-2605.

Ivanov, V., Sheshukov, A., Zhou, W., Zhu, M., & Wang, J. (2023a). Lpteg-trees1: Hydrometeorological, subsurface, and snow data in Western Siberia near Salekhard of Yamal-Nenets Autonomous District, Russia, 2018–2021. Arctic Data Center. https://doi.org/10.18739/A2NZ80R6H

Ivanov, V., Sheshukov, A., Zhou, W., Zhu, M., & Wang, J. (2023b). Lpteg-trees2: Hydrometeorological, subsurface, and snow data in Western Siberia near Salekhard of Yamal-Nenets Autonomous District, Russia, 2018–2021. Arctic Data Center. https://doi.org/10.18739/A2J960B6W
Ivanov, V., Sheshukov, A., Zhou, W., Zhu, M., & Wang, J. (2023c). Lpteg-tundra2: Hydrometeorological, subsurface, and snow data in Western

Siberia near Salekhard of Yamal-Nenets Autonomous District, Russia, 2018–2021. Arctic Data Center. https://doi.org/10.18739/A2SQ8QK0W Jorgenson, M. T., Shur, Y. L., & Pullman, E. R. (2006). Abrupt increase in permafrost degradation in Arctic Alaska. Geophysical Research Letters, 33(2), L02503. https://doi.org/10.1029/2005g1024960

Kudryavtsev, V., Garagulya, L., & Melamed, V. (1977). Fundamentals of frost forecasting in geological engineering investigations. (Tech. Rep.). Cold Regions Research and Engineering Laboratory.

Ladanyi, B., & Andersland, O. (2004). Frozen ground engineering. Wiley.

Li, L., Yu, Y., Tang, Y., Lin, P., Xie, J., Song, M., et al. (2020). The flexible global ocean-atmosphere-land system model grid-point version 3 (FGOALS-g3): Description and evaluation. *Journal of Advances in Modeling Earth Systems*, 12(9), e2019MS002012. https://doi.org/10.1029/2019ms002012

Li, R., Xie, J., Xie, Z., Gao, J., Jia, B., Qin, P., et al. (2021). Simulated spatial and temporal distribution of freezing and thawing fronts in CAS-FGOALS-g3. Journal of Advances in Modeling Earth Systems, 13(10), e2020MS002152. https://doi.org/10.1029/2020ms002152

Li, X., & Koike, T. (2003). Frozen soil parameterization in SiB2 and its validation with GAME-Tibet observations. *Cold Regions Science and Technology*, 36(1–3), 165–182. https://doi.org/10.1016/s0165-232x(03)00009-0

Lunardini, V. J. (1981). Heat transfer in cold climates. Van Nostrand Reinhold Company.

Mamode, M. (2013). Two phase Stefan problem with boundary temperature conditions: An analytical approach. SIAM Journal on Applied Mathematics, 73(1), 460–474. https://doi.org/10.1137/110852474

McGaw, R., SI, O., & Ng, E1. (1978). Thermal properties and regime of wet tundra soils at Barrow, Alaska. In *Proceedings of the third international conference on permafrost* (pp. 47–53). National Research Council of Canada.

Miller, R. (1980). Freezing phenomena in soil. In D. Hillel (Ed.), Applications of soil physics. Academic Press.

Nelson, F., Outcalt, S., Goodwin, C., & Hinkel, K. (1985). Diurnal thermal regime in a peat-covered palsa, Toolik Lake, Alaska. *Arctic*, 38(4), 310–315. https://doi.org/10.14430/arctic2150

Nelson, F., Shiklomanov, N., Mueller, G., Hinkel, K., Walker, D., & Bockheim, J. (1997). Estimating active-layer thickness over a large region: Kuparuk River Basin, Alaska, USA. Arctic and Alpine Research, 29(4), 367–378. https://doi.org/10.2307/1551985

ZHU ET AL. 12 of 13

- Obu, J., Westermann, S., Bartsch, A., Berdnikov, N., Christiansen, H. H., Dashtseren, A., et al. (2019). Northern hemisphere permafrost map based on ttop modelling for 2000–2016 at 1 km2 scale. *Earth-Science Reviews*, 193, 299–316. https://doi.org/10.1016/j.earscirev.2019.04.023
- Ochsner, T. E., & Baker, J. M. (2008). In situ monitoring of soil thermal properties and heat flux during freezing and thawing. Soil Science Society of America Journal, 72(4), 1025–1032. https://doi.org/10.2136/sssaj2007.0283
- Oelke, C., Zhang, T., Serreze, M. C., & Armstrong, R. L. (2003). Regional-scale modeling of soil freeze/thaw over the Arctic drainage basin. *Journal of Geophysical Research*, 108(D10), 4314. https://doi.org/10.1029/2002jd002722
- Oleson, K., Lawrence, D. M., Bonan, G. B., Drewniak, B., Huang, M., Koven, C. D., & Yang, Z.-L. (2013). Technical description of version 4.5 of the community land model (CLM) (Tech. Rep. Nos. NCAR/TN-503+STR). https://doi.org/10.5065/D6RR1W7M
- Outcalt, S. I., Nelson, F. E., & Hinkel, K. M. (1990). The zero-curtain effect: Heat and mass transfer across an isothermal region in freezing soil. Water Resources Research, 26(7), 1509–1516. https://doi.org/10.1029/wr026i007p01509
- Overduin, P. P., & Kane, D. (2006). Frost boils and soil ice content: Field observations. *Permafrost and Periglacial Processes*, 17(4), 291–307. https://doi.org/10.1002/ppp.567
- Overpeck, J., Hughen, K., Hardy, D., Bradley, R., Case, R., Douglas, M., et al. (1997). Arctic environmental change of the last four centuries. Science, 278(5341), 1251–1256. https://doi.org/10.1126/science.278.5341.1251
- Patterson, D., & Smith, M. (1981). The measurement of unfrozen water content by time domain reflectometry: Results from laboratory tests. Canadian Geotechnical Journal, 18(1), 131–144. https://doi.org/10.1139/t81-012
- Riseborough, D., Shiklomanov, N., Etzelmüller, B., Gruber, S., & Marchenko, S. (2008). Recent advances in permafrost modelling. *Permafrost*
- and Periglacial Processes, 19(2), 137–156. https://doi.org/10.1002/ppp.615
 Robinson, S. D., Turetsky, M. R., Kettles, I. M., & Wieder, R. K. (2003). Permafrost and peatland carbon sink capacity with increasing latitude. In
- Proceedings of the 8th international conference on permafrost (Vol. 2, pp. 965–970).

 Romanovsky, V., & Osterkamp, T. (1997). Thawing of the active layer on the coastal plain of the Alaskan Arctic. Permafrost and Periglacial
- Processes, 8(1), 1–22. https://doi.org/10.1002/(sici)1099-1530(199701)8:1<1::aid-ppp243>3.3.co;2-1
 Romanovsky, V. E., Smith, S. L., & Christiansen, H. H. (2010). Permafrost thermal state in the polar northern hemisphere during the international
- polar year 2007–2009: A synthesis. Permafrost and Periglacial Processes, 21(2), 106–116. https://doi.org/10.1002/ppp.689
- Schuur, E. A., McGuire, A. D., Schädel, C., Grosse, G., Harden, J. W., Hayes, D. J., et al. (2015). Climate change and the permafrost carbon feedback. *Nature*, 520(7546), 171–179. https://doi.org/10.1038/nature14338
- Sellers, P., Randall, D., Collatz, G., Berry, J., Field, C., Dazlich, D., et al. (1996). A revised land surface parameterization (SiB2) for atmospheric GCMs. Part I: Model formulation. *Journal of Climate*, 9(4), 676–705. https://doi.org/10.1175/1520-0442(1996)009<0676:arlspf>2.0.co;2
- Serreze, M., Walsh, J. E., Chapin III, F. S., Osterkamp, T., Dyurgerov, M., Romanovsky, V., et al. (2000). Observational evidence of recent change in the northern high-latitude environment. Climatic Change, 46(1/2), 159–207. https://doi.org/10.1023/a:1005504031923
- Streletskiy, D. A., Shiklomanov, N. I., & Nelson, F. E. (2012). Permafrost, infrastructure, and climate change: A GIS-based landscape approach to geotechnical modeling. *Arctic Antarctic and Alpine Research*, 44(3), 368–380. https://doi.org/10.1657/1938-4246-44.3.368
- Van Everdingen, R. (1998). Multi-language glossary of permafrost and related ground-ice terms, revisado en mayo de 2005. National Snow and Ice Data Center/World Data Center for Glaciology.
- Vuik, C. (1993). Some historical notes about the Stefan problem. Delft University of Technology Delft.
- Walvoord, M. A., & Kurylyk, B. L. (2016). Hydrologic impacts of thawing permafrost—A review. Vadose Zone Journal, 15(6), 1–20. https://doi.org/10.2136/vzj2016.01.0010
- Wang, J., & Bras, R. (2011). A model of evapotranspiration based on the theory of maximum entropy production. Water Resources Research, 47(3), W03521. https://doi.org/10.1029/2010wr009392
- Wang, J., & Bras, R. L. (2009). A model of surface heat fluxes based on the theory of maximum entropy production. *Water Resources Research*, 45(11), W11422. https://doi.org/10.1029/2009wr007900
- Wang, Z.-H., & Bou-Zeid, E. (2012). A novel approach for the estimation of soil ground heat flux. Agricultural and Forest Meteorology, 154, 214–221. https://doi.org/10.1016/j.agrformet.2011.12.001
- Yang, J., & Wang, Z.-H. (2014). Land surface energy partitioning revisited: A novel approach based on single depth soil measurement. Geophysical Research Letters, 41(23), 8348–8358. https://doi.org/10.1002/2014g1062041
- Yi, Y., Kimball, J. S., Chen, R. H., Moghaddam, M., Reichle, R. H., Mishra, U., et al. (2018). Characterizing permafrost active layer dynamics and sensitivity to landscape spatial heterogeneity in Alaska. The Cryosphere, 12(1), 145–161. https://doi.org/10.5194/tc-12-145-2018

ZHU ET AL. 13 of 13